Determination of Solvent Systems for Blade Coating Thin Film Photovoltaics

*Jeffrey G. Tait, Tamara Merckx, Wenqi Li, Cindy Wong, Robert Gehlhaar, David Cheyns, Mathieu Turbiez, and Paul Heremans**

With lab-scale solution-processed thin film photovoltaic (TFPV) devices attaining market relevant efficiencies, the demand for environmentally friendly and scalable deposition techniques is increasing. Replacing toxic halogenated solvents is a priority for the industrialization of solution-processed TFPV. In this work, a generalized five-step process is presented for fabricating high-performance devices from nonhalogenated inks. Resulting from this process, several new solvent systems are introduced based on thiophene, tetralin, 1,2,4-trimethylbenzene, *o*-xylene, and anisole for blade coating of three different diketopyrrolopyrrole-based (pDPP5T-2, pPDPP5T-2S, and P390) bulk heterojunctions applied in organic photovoltaic devices. Devices based on pDPP5T-2S and P390 attain 5.6% and 6.1% efficiency, respectively, greater than the efficiency either material reached when processed from the halogenated solvent system commonly used. These processes are implemented without post-deposition annealing treatments or additives. The Hansen solubility parameters of the pDPP5T-2 material are obtained, and are used, along with wettability data on a variety of substrates, to determine optimum solvent combinations and ratios for deposition. This generalized five-step process results in new nonhalogenated solvent pathways for the scalable deposition of thin film photovoltaic materials.

1. Introduction

Thin film photovoltaics (TFPV) have reached efficiencies, 10.8% for single-junction polymer organic photovoltaics (OPV),[1] 12% for small molecule evaporated OPV,[2] and 20% for perovskite-based devices, sufficient for commercialization.[3] One of the limiting factors in the industrial uptake of solution-processed TFPV is the use of toxic and halogenated solvents to dissolve the photoactive blend of materials. Furthermore, the deposition technique typically used for lab-scale solution-processed TFPV, spin coating, is not transferable to an industrial production setting.[4–6] Transitioning to nonhalogenated solvents affords a more environmentally friendly and less toxic approach, while blade coating offers a precise and reliable linear deposition technique that can be scaled from lab to fab.[7–14]

Blade coating is a large area applicable, linear deposition technique used in roll-to-roll and sheet-to-sheet coating industries.[4,15–17] A blade, in near-contact with the underlying substrate, spreads a droplet of ink over a substrate, optimally resulting in a smooth and uniform coating, free of pinholes and ribbing. Blade height, blade speed, and substrate temperature are some of the key intrinsic deposition parameters, while ink composition is a determining factor for deposition results, solubility, and wettability.

The Hansen solubility parameters (HSP) describe the properties of solutes, solvents, and solvent systems, and enable a theoretical description of the solubility of materials.[18,19] Three parameters represent the polar, hydrogen, and dispersion components of interaction for both materials and solvents, where similar-valued materials are more likely to dissolve each other than dissimilar-valued materials. The HSP space of solubility for a solute may be approximated by an ellipsoidal volume where solvent systems with a combined parameter value within this volume dissolve the solute, while those systems with a value outside the ellipsoid do not dissolve the solute. The HSP for a material are determined by measuring the material solubility in a variety of solvents with known solubility parameters and by fitting an ellipsoid to the HSP for equal solute concentrations. Thus, the HSP are dependent on the threshold of solubility desired, shifting with the concentration limits of the foreseen application. This selection method has been described in several studies for the determination of solvents for organic photovoltaic materials.[7,12,20,21]

Nonhalogenated solvents are one step toward industrially viable printing of solution-processed TFPV.[7–14] Several studies have reported potential replacements for halogenated solvents that are commonly used in OPV fabrication; however,

J. G. Tait, W. Li, Prof. P. Heremans
KU Leuven
Kasteelpark Arenberg 10, Leuven B-3001, Belgium
J. G. Tait, Dr. T. Merckx, W. Li, C. Wong, Dr. R. Gehlhaar, Dr. D. Cheyns, Prof. P. Heremans
IMEC, Kapeldreef 75, Leuven B-3001, Belgium
E-mail: heremans@imec.be
C. Wong
The Cooper Union
30 Cooper Sq., New York, NY 10003, USA
Dr. M. Turbiez
BASF Schweiz AG
Schwarzwaldallee 215, CH-4002 Basel, Switzerland

DOI: 10.1002/adfm.201501039

most require less desirable additives or post-deposition treatments.[7–10,13] An optimal replacement removes these processes, while decreasing the toxicity of the inks. It must be noted that "nonhalogenated" does not equate to "nontoxic"; however, conclusive literature on the toxicological and environmental impact of industrially uncommon solvents is deficient. Beyond the toxicity of the solvents used, several further issues must also addressed for commercialization, including the cost of materials and electrodes,[22,23] device reliability,[24,25] and the potential need for replacement of lead in the emerging field of perovskite-based TFPV.[26,27]

In this work, we present a generalized five-step process for fabricating high performance TFPV from nonhalogenated inks:

1. Compile solvent list and remove toxic/halogenated solvents.
2. Test wettability of solvents on underlying substrate to be implemented.
3. Determine HSP for material.
4. Perform first selection of potential solvent combinations with complimentary HSP for solubility, miscibility, and drying time.
5. Optimize deposition for uniform coating and high-performance devices, leading to a final selection of solvent combination, solution composition, and deposition parameters.

This methodology can be applied to the processing of any type of solution-processed device, and is implemented for OPV devices in this work. Using this five-step process, we describe new nonhalogenated solvent systems, based on thiophene, tetralin, 1,2,4-trimethylbenzene, *o*-xylene, and anisole for blade coating several diketopyrrolopyrrole-based (pDPP5T-2, pDPP5T-2S, P390) OPV devices (chemical structure shown in **Figure 1**).[28,29] These solvent systems are determined using a full investigation of the HSP of the least soluble material, pDPP5T-2. Contact angle measurements reveal the potential for coating the inks on typical underlying layers, including TiO_2, MoO_3, poly [(9,9-bis(3′-(*N*,*N*-dimethylamino)propyl)-2,7-fluorene)-alt-2,7-(9,9-dioctylfluorene)] (PFN-2), and ZnO. Fabricated devices are optimized for photoactive layer thickness and coating conditions to achieve devices with comparable performance to those with halogenated solvents. This high performance was attained without the need for additives or post-deposition treatments.

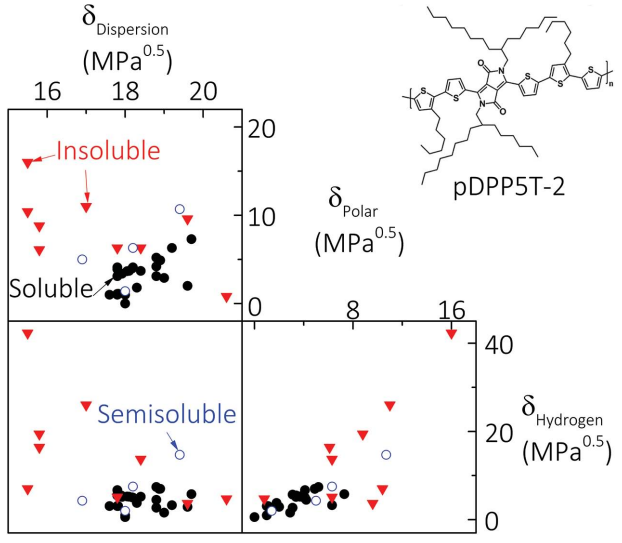

Figure 1. Hansen solubility parameter space, represented by 2D projections onto the dispersive, polar, and hydrogen dimensions, represented by black symbols for good solvents (>2 g L^{-1}), blue symbols for semi-solvents (1–2 g L^{-1}), and red symbols for nonsolvents (<1 g L^{-1}). The good solvents are clustered around ranges of $\delta_{dispersive} = 19 \pm 1$ $MPa^{0.5}$, $\delta_{polar} = 3 \pm 2$ $MPa^{0.5}$, and $\delta_{hydrogen} = 2 \pm 2$ $MPa^{0.5}$.

2. Results and Discussion

2.1. Wetting-Contact Angle

The implemented solvent system must wet the substrate surface to achieve smooth, uniform, and reproducible films from blade coating. Contact angle measurements reveal the wettability on each of the evaporated MoO_3 and solution-processed TiO_2, ZnO, and PFN-2 layers (**Table 1**). Multiple successive measurements were carried out to ensure a steady-state value. Some polar solvents, e.g., water, result in larger error in their measurement due to degradation of the underlying layer. In this study, TiO_2 was selected as the underlying transport layer in the final device structure due to its solution deposition at room temperature, its high surface energy ($\gamma_{total} = 59.7$ N m^{-1}, $\gamma_{polar} = 23.1$ N m^{-1}, and $\gamma_{dispersive} = 36.7$ N m^{-1}), and its known device performance with pDPP5T-2.[28]

2.2. Hansen Solubility Parameters

The HSP for pDPP5T-2 are $\delta_{dispersive} = 19 \pm 1$ $MPa^{0.5}$, $\delta_{polar} = 3 \pm 2$ $MPa^{0.5}$, and $\delta_{hydrogen} = 2 \pm 2$ $MPa^{0.5}$, determined with its solubility limits (Table 1). The solubility limits were determined by progressively diluting solutions until no aggregates remained at room temperature, after which a film could be coated without particles. Figure 1 represents the 3D HSP space by its 2D projections of the hydrogen, polar, and dispersion dimensions for solvents and nonsolvents. The chemical structure of pDPP5T-2 is also shown in Figure 1. A more comprehensive list of HSP for each solvent is included in Table S1 (Supporting Information).

When dissolved in a variety of solvents, pDPP5T-2 displays a large absorption spectrum dependence on the solvent, ranging from red to blue. A photograph of a selection of solvents is shown in Figure S1 (Supporting Information). Normalized UV–vis absorption spectra for pDPP5T-2 in solvents further used in this study are depicted in **Figure 2**. All measured solutions were dilute and free of aggregates. Chloroform and thiophene show an absorption peak at 750 nm, suggesting an interaction of polymer chains.

Solvent systems of chloroform/*ortho*-dichlorobenzene, thiophene/tetralin, thiophene/1,2,4-trimethylbenzene, thiophene/anisole, *o*-xylene/tetralin, and *o*-xylene/anisole provide proper solubility of pDPP5T-2 and coatability on TiO_2. These systems were determined with the following criteria: individual solvent HSP on opposing sides of the pDPP5T-2 HSP center, low boiling points for both solvents, small contact angle on TiO_2,

Table 1. Contact angles of pure solvents on glass substrates coated with typical interfacial layers and pDPP5T-2 solubility range.

Solvent	Contact angle[a] [°]				pDPP5T-2 solubility [g L^{-1}]
	TiO_2	MoO_3	PFN-2	ZnO	
1,2,3-Trimethylbenzene	0	0	0	6	2–4
1,2,4-Trimethylbenzene	0	0	0	0	2–4
1,3,5-Trimethylbenzene	0	0	0	15	2–4
Acetone	0	0	12	0	0
Acetophenone	4	6	21	3	<1
Anisole	0	0	15	6	>4
Benzyl alcohol	0	15	16	23	0
Chloroform	12	9	10	9	>4
Cyclohexanone	0	5	14	0	–
Diiodomethane	35	38	49	43	–
Ethanol	0	0	14	0	0
Ethylbenzene	4	0	5	5	–
Ethylene glycol	31	23	44	41	0
Hexadecane	12	24	7	10	–
Indane	3	0	18	5	2–4
Isopropanol	0	0	0	0	0
m-Xylene	0	0	0	22	2–4
o-Xylene	0	3	0	0	2–4
Ortho-Dichlorobenzene	5	11	22	8	2–4
p-Xylene	0	0	0	0	2–4
Salicylaldehyde	2	7	26	27	–
Terpineol	17	18	15	12	–
Tetralin	0	7	9	6	2–4
Thiophene	9	9	12	11	>4
Toluene	0	0	0	0	<1
Veratrole	14	12	26	9	<1
Water	27	21	104	29	0

[a]Contact angles of 0° represent complete wetting, with angles too small to reliably measure.

and miscibility of the two solvents. Thiophene is a primary solvent for several solvent systems due to its strong single solvent capabilities, while *o*-xylene provides contrasting HSP to several other solvents. The volume ratios for each solvent system have combined HSP near the center of the pDPP5T-2 ellipsoid. Furthermore, within the soluble HSP ellipsoid, the solvents and their ratios were chosen to provide a Marangoni flow, alongside the convection driven flow, to reduce the coffee ring effect.[30–32] Marangoni flows result from a gradient in surface tension in a liquid, where the volume of higher surface tension effectively "pulls" the liquid in a low surface tension volume toward it.[31]

The three polymers—pDPP5T-2, pDPP5T-2S, and P390—are designed to be progressively more soluble. The photoactive component of each includes a diketopyrrolopyrrole surrounded by five thiophene units. The pDPP5T-2S has a lower molecular weight (44 500 g mol^{-1}) than that of pDPP5T-2 (47 000 g mol^{-1}).

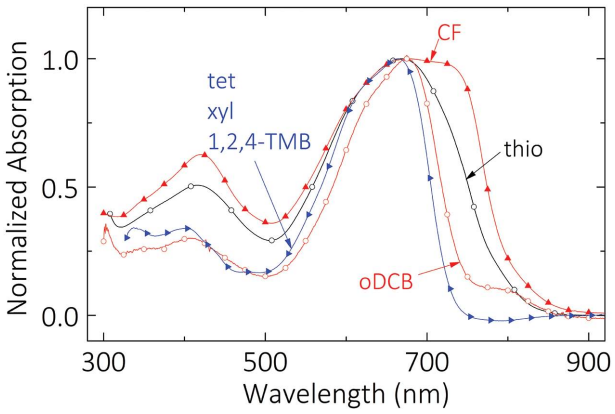

Figure 2. Normalized absorption spectra for dilute solutions of pDPP5T-2. The solvents shown are chloroform (CF), *ortho*-dichlorobenzene (oDCB), thiophene (thio), tetralin (tet), xylene (xyl), and 1,2,4-trimethylbenzene (1,2,4-TMB).

When blade coated, the solubility limit of pDPP5T-2 in the above systems did not provide the thickness required for efficient device performance.[28] Low solubility inks may be implemented with techniques that require lower concentrations, such as spray coating.[33] Both pDPP5T-2S and P390 have solubility limits ≈10 g L^{-1} in chloroform, *ortho*-dichlorobenzene, thiophene, tetralin, 1,2,4-trimethylbenzene, anisole, *o*-xylene, and the solvent systems of each. Thus, the HSP ellipsoid of these two materials envelopes that of pDPP5T-2. Both of these materials reach layer thicknesses up to 300 nm when blade coated from the same solvent systems as pDPP5T-2.

2.3. Device Fabrication

Blade coating offers an abundance of parameters to be screened for the optimum deposition process. The blade height, blade speed, substrate temperature, and the ratio of the two solvents in the system were adjusted to attain uniform and smooth layer formation. Higher blade height and higher blade speed produce thicker films, while substrate temperature is effective at ensuring a high enough solvent evaporation rate to complete layer formation in a short time. For the solvent systems used in this study, elevated temperatures had no effect on device performance, nor film morphology. Thus, room temperature depositions were used with all inks. Blade coating from the pure solvents used in this study does not provide uniform films, due to the film dewetting whilst drying.

Full OPV devices with a structure of ITO/TiO_2/pDPP5T-2:[70]PCBM/MoO_3/Ag were fabricated, with a blade-coated photoactive layer deposited from the solvent systems listed in **Table 2**. The top MoO_3/Ag electrodes were evaporated without a post-deposition treatment to the photoactive layer. The external quantum efficiency (EQE) spectrum for the pDPP5T-2 device deposited from CF:ODCB is approximately 60% over the full absorption spectrum (Figure S2, Supporting Information). In the case of the nonhalogenated solvent systems, the low solubility of pDPP5T-2 limits the performance. Filtered solutions of pDPP5T-2:[70]PCBM were deposited, effectively coating at the highest concentration of pDPP5T-2 possible, resulting in

Table 2. Device performance for OPV devices with blade-coated donor:[70]PCBM photoactive layers.

Solvent system	Donor material	Solvent ratio [v/v%]	η [%]	FF [%]	J_{SC} (EQE) [mA cm^{-2}]	V_{OC} [mV]	PAL thickness [nm]
Chloroform/*ortho*-dichlorobenzene	pDPP5T-2	80/20	6.3	67	17.3 (17.1)	540	80
Thiophene/tetralin	pDPP5T-2	80/20	0.7	59	2.3 (–)	550	130
Thiophene/1,2,4-trimethylbenzene	pDPP5T-2	90/10	0.7	62	2.0 (–)	570	100
o-Xylene/tetralin	pDPP5T-2	97/3	0.6	60	1.8 (–)	540	66
Chloroform/*ortho*-dichlorobenzene	pDPP5T-2S	80/20	4.9	63	14.2 (13.6)	550	106
Thiophene/tetralin	pDPP5T-2S	80/20	4.9	65	13.6 (13.6)	550	88
Thiophene/1,2,4-trimethylbenzene	pDPP5T-2S	90/10	4.9	64	13.7 (13.2)	560	109
Thiophene/anisole	pDPP5T-2S	90/10	4.5	55	14.8 (13.3)	560	110
o-Xylene/tetralin	pDPP5T-2S	97/3	5.6	67	15.5 (15.2)	540	90
o-Xylene/anisole	pDPP5T-2S	97/3	2.2	57	6.9 (7.8)	550	103
Chloroform/*ortho*-dichlorobenzene	P390	80/20	5.1	61	14.6 (14.5)	560	120
Thiophene/tetralin	P390	80/20	6.1	65	17.5 (17.2)	550	129
Thiophene/1,2,4-trimethylbenzene	P390	90/10	5.8	65	15.3 (15.4)	570	70
Thiophene/anisole	P390	90/10	4.9	62	14.5 (14.1)	550	102
o-Xylene/tetralin	P390	97/3	4.9	61	14.8 (–)	550	68
o-Xylene/anisole	P390	97/3	3.2	59	9.9 (–)	560	60

suitable thickness for devices but a high [70]PCBM loading of approximately 90 wt%. The pDPP5T-2 devices from nonhalogenated inks achieve suitable open circuit voltage (V_{OC}) and fill factor (FF) for pDPP5T-2.[28] These devices are limited in short circuit current density (J_{SC}) due to the low absorption of [70]PCBM relative to pDPP5T-2. Reference pDPP5T-2 devices from chloroform (CF): *ortho*-dichlorobenzene (ODCB) inks give a high performance of 6.3% efficiency at a photoactive layer thickness of 80 nm.

Devices with the same architecture as above but with pDPP5T-2 replaced with either pDPP5T-2S or P390 display high performance with nonhalogenated solvent systems. The high performance is owing to the high solubility and ensuing layers of sufficient thickness (Table 2). A study of P390-based device performance as a function of photoactive layer thickness for devices indicates optimum current production at 90 and 230 nm, regardless of the solvent system (**Figure 3**). This range of layer thickness was obtained by varying the blade speed and height. These trends concur with the literature for pDPP5T-2 based on the same device architectures.[28] Unfortunately, the second interference peak in current production at 230 nm cannot be utilized for high-performance devices due to the rapid drop in FF, limited by charge carrier collection in thick devices (Figure S3, Supporting Information).

Optimized pDPP5T-2S and P390 devices coated from nonhalogenated inks achieve comparable performance to those deposited from optimized halogenated inks. The device performance metrics (Table 2) indicate high performance with most of the nonhalogenated inks. The corresponding current density versus voltage plots and EQE spectra are presented in Figure S2 (Supporting Information). The pDPP5T-2S performed the best in xylene:tetralin with 5.6% efficiency, and P390 had the highest efficiency in thiophene:tetralin with 6.1% efficiency. Due to slight differences in solubility and drying conditions, these two similar materials show high performance in the same solvent systems, but peak performance in different inks. A nonhalogenated solvent system cannot be universal for a family of materials, but must be empirically tested to provide the best resultant morphology.

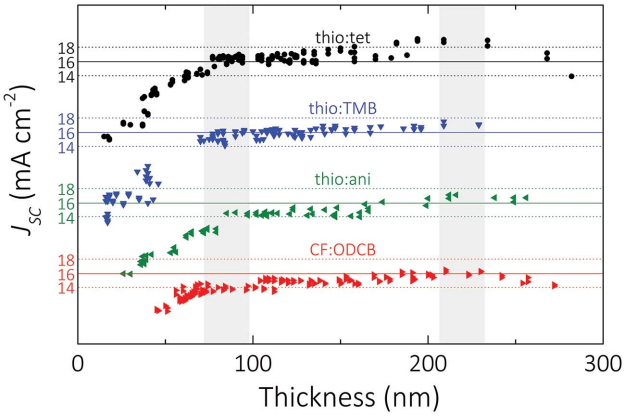

Figure 3. A comparison of current production in blade coated P390 devices for each solvent system showing identical maxima with thicknesses determined by optical interference. The short circuit current density (J_{SC}) versus photoactive layer thickness plots for different solvents systems are presented in order of decreasing current production: thiophene:tetralin (black circles), thiophene:1,2,4-trimethylbenzene (blue down-facing triangles), thiophene:anisole (left-facing triangles), and chloroform: *ortho*-dichlorobenzene (red right-facing triangles). The optical interference maxima, as determined from simulations, are indicated by grey ranges around thicknesses of 90 and 230 nm. Equal valued horizontal lines of the J_{SC} are drawn for each system to indicate relative differences.

3. Conclusion

A five-step process was presented to optimize the performance of solution-processed photovoltaic devices coated from nonhalogenated inks. First, known toxic and dangerous solvents are filtered out of the compilation of potential solvents. It must be noted that several of the nonhalogenated solvents used in this study lack sufficient literature on their toxicological and environmental impacts, representing a potential for advancement of the knowledge of the coating community. Second, a selection of solvents is tested for wettability on the underlying layer determined by the device architecture to be implemented. Third, the Hansen solubility parameters for the material system are found, and the complementary solvents on the opposing sides of the material HSP are chosen. Next, ratios of the multisolvent system with the combined HSP within the solubility space of the materials are adjusted to blade coat smooth and uniform films. Last, blade-coating parameters, such as blade speed, blade height, and substrate temperature, were optimized for peak device performance.

Using this process, nonhalogenated solvent systems based on thiophene, tetralin, 1,2,4-trimethylbenzene, anisole, and *o*-xylene are developed for three photoactive materials based on diketopyrrolopyrrole surrounded by five thiophenes (pDPP5T-2, pDPP5T-2S, and P390). A selection of solvents is tested for wettability on solution-processed TiO_2, MoO_3, PFN-2, and ZnO layers, while the Hansen solubility parameters for pDPP5T-2 are found to be $\delta_{dispersive} = 19 \pm 1$ MPa$^{0.5}$, $\delta_{polar} = 3 \pm 2$ MPa$^{0.5}$, and $\delta_{hydrogen} = 2 \pm 2$ MPa$^{0.5}$. The higher solubility of pDPP5T-2S and P390 in the same solvents results in a solubility ellipsoid enveloping that of pDPP5T-2. This overlap enables the use of the same solvent systems for all three materials. Devices from nonhalogenated inks achieve higher performance than those coated from the archetypal halogenated solvent system; P390 and pDPP5T-2S devices attained 6.1% and 5.6%, respectively, with nonhalogenated solvents, compared to 5.1% and 4.9%, respectively, with halogenated solvent systems. This general five-step process demonstrates the applicability of Hansen solubility parameters to a range of materials in a family of polymers, showing a new pathway for the industrial-scale deposition of TFPV materials with more environmentally friendly inks.

4. Experimental Section

Materials: The patterned 3 × 3 cm glass/ITO substrates were purchased from Colorado Concepts (R_S = 20 Ω □$^{-1}$). The pDPP5T-2 (M_w = 47 000 g mol^{-1}, PDI = 2.2, Lot: GKS1-001), pDPP5T-2S (M_w = 44 500 g mol^{-1}, PDI = 2.3, Lot: 2440-151R2), and P390 were synthesized by BASF, while [6,6]-phenyl-C71-butyric acid ([70]PCBM) (99%) was purchased from Nano-C. All solvents were purchased from Sigma-Aldrich.

Device Fabrication: Substrates were cleaned with successive ultrasonic baths in detergent, deionized water, acetone, and isopropanol. All device fabrication steps were carried out in an N_2 environment. TiO_2 sol–gel in ethanol was spin coated to give 5 nm thick layers. Layers of ZnO were spun coat from a ZnO precursor (zinc acetate dehydrate dissolved in 2-ethoxyethanol, ethanolamine, and ethanol) and annealed at 300 °C. PFN-2 was spin coated as described in the literature.[34] Solutions of the DPP donor and [70]PCBM acceptor in the solvent systems were mixed and stirred at 80 °C, and cooled to room temperature before blade coating. Blade coating was performed with a film applicator Multicator 411 on a Coatmaster 510 (Erichsen) with coating speeds between 20 and 80 mm s^{-1}. The substrates were held at either 20 or 60 °C during deposition. The top contacts of MoO_3 and Ag were thermally evaporated at a pressure of 10^{-5} Pa to thicknesses of 10 and 150 nm, respectively.

Characterization: The contact angle measurements were performed with an OCA-20 contact angle measurement system (DataPhysics GmbH). Solvents were tested for solubility limits by trying to dissolve the polymer at high concentration and elevated temperature. The solution was then diluted until no aggregates were found and layers were coated without particles. Atomic force microscopy (AFM) images were recorded on a Picoscan PicoSPM LE scanning probe microscope operated in tapping mode. Film thicknesses were measured by a Dektak D150 (Veeco Instruments) surface profilometer. The current density versus voltage measurements were done with a Keithley 2602A Source-Measure Unit and an Abet solar simulator producing 100 mW cm^{-2} AM1.5G illumination. External quantum efficiency was measured with coupled and monochromated Xe and quartz halogen lamps calibrated by a Si photodiode.

Supporting Information

Supporting Information is available from the Wiley Online Library or from the author.

Acknowledgements

This work received partial funding from the European Commission via the 7th framework project "ArtESun" (NMP3-SL-2013-604397) and from the Flemish Government: Department Economy, Science and Innovation. J.G. Tait acknowledges partial funding from the Natural Sciences and Engineering Research Council of Canada. The figures were converted to color on June 10, 2015.

Received: March 16, 2015
Revised: April 8, 2015
Published online: April 30, 2015

[1] Y. Liu, J. Zhao, Z. Li, C. Mu, W. Ma, H. Hu, K. Jiang, H. Lin, H. Ade, H. Yan, *Nat. Commun.* **2014**, *5*, 1.
[2] Heliatek Press Release, January 16, **2013**.
[3] M. A. Green, K. Emery, Y. Hishikawa, W. Warta, E. D. Dunlop, *Prog. Photovoltaics Res. Appl.* **2015**, *23*, 1.
[4] F. C. Krebs, *Sol. Energy Mater. Sol. Cells* **2009**, *93*, 394.
[5] R. Søndergaard, M. Hösel, D. Angmo, T. T. Larsen-Olsen, F. C. Krebs, *Mater. Today* **2012**, *15*, 36.
[6] Y. Galagan, I. G. de Vries, A. P. Langen, R. Andriessen, W. J. H. Verhees, S. C. Veenstra, J. M. Kroon, *Chem. Eng. Process. Process Intensif.* **2011**, *50*, 454.
[7] C.-D. Park, T. A. Fleetham, J. Li, B. D. Vogt, *Org. Electron.* **2011**, *12*, 1465.
[8] K.-S. Chen, H.-L. Yip, C. W. Schlenker, D. S. Ginger, A. K.-Y. Jen, *Org. Electron.* **2012**, *13*, 2870.
[9] B. R. Aïch, S. Beaupré, M. Leclerc, Y. Tao, *Org. Electron.* **2013**, *15*, 543.
[10] G.-H. Lim, J.-M. Zhuo, L.-Y. Wong, S.-J. Chua, L.-L. Chua, P. K. H. Ho, *Org. Electron.* **2014**, *15*, 449.
[11] A. Lange, W. Schindler, M. Wegener, K. Fostiropoulos, S. Janietz, *Sol. Energy Mater. Sol. Cells* **2013**, *109*, 104.
[12] I. Burgués-Ceballos, F. Machui, J. Min, T. Ameri, M. M. Voigt, Y. N. Luponosov, S. A. Ponomarenko, P. D. Lacharmoise, M. Campoy-Quiles, C. J. Brabec, *Adv. Funct. Mater.* **2014**, *24*, 1449.
[13] K. Tada, M. Onoda, *Sol. Energy Mater. Sol. Cells* **2012**, *100*, 246.
[14] K. Tada, *Sol. Energy Mater. Sol. Cells* **2013**, *108*, 82.

[15] N. Li, D. Baran, K. Forberich, F. Machui, T. Ameri, M. Turbiez, M. Carrasco-Orozco, M. Drees, A. Facchetti, F. C. Krebs, C. J. Brabec, *Energy Environ. Sci.* **2013**, *6*, 3407.
[16] Y.-H. Chang, S.-R. Tseng, C.-Y. Chen, H.-F. Meng, E.-C. Chen, S.-F. Horng, C.-S. Hsu, *Org. Electron.* **2009**, *10*, 741.
[17] B. Schmidt-Hansberg, M. Sanyal, M. F. G. Klein, M. Pfaff, N. Schnabel, S. Jaiser, A. Vorobiev, E. Müller, A. Colsmann, P. Scharfer, D. Gerthsen, U. Lemmer, E. Barrena, W. Schabel, *ACS Nano* **2011**, *5*, 8579.
[18] C. M. Hansen, *Hansen Solubility Parameters: A User's Handbook*, 2nd ed., CRC Press, Boca Raton, FL **2007**.
[19] C. M. Hansen, A. L. Smith, *Carbon N. Y.* **2004**, *42*, 1591.
[20] F. Machui, S. Langner, X. Zhu, S. Abbott, C. J. Brabec, *Sol. Energy Mater. Sol. Cells* **2012**, *100*, 138.
[21] B. Walker, A. Tamayo, D. T. Duong, X.-D. Dang, C. Kim, J. Granstrom, T.-Q. Nguyen, *Adv. Energy Mater.* **2011**, *1*, 221.
[22] J. G. Tait, M. De Volder, D. Cheyns, P. Heremans, B. Rand, *Nanoscale* **2015**, *7*, 7259.
[23] Z. Li, S. A. Kulkarni, P. P. Boix, E. Shi, A. Cao, K. Fu, S. K. Batabyal, J. Zhang, Q. Xiong, L. H. Wong, N. Mathews, S. G. Mhaisalkar, *ACS Nano* **2014**, *8*, 6797.
[24] E. Voroshazi, B. Verreet, T. Aernouts, P. Heremans, *Sol. Energy Mater. Sol. Cells* **2011**, *95*, 1303.
[25] B. J. Worfolk, T. C. Hauger, K. D. Harris, D. A. Rider, J. A. M. Fordyce, S. Beaupré, M. Leclerc, J. M. Buriak, *Adv. Energy Mater.* **2012**, *2*, 361.
[26] Y. Takahashi, R. Obara, Z.-Z. Lin, Y. Takahashi, T. Naito, T. Inabe, S. Ishibashi, K. Terakura, *Dalton Trans.* **2011**, *40*, 5563.
[27] N. K. Noel, S. D. Stranks, A. Abate, C. Wehrenfennig, S. Guarnera, A. Haghighirad, A. Sadhanala, G. E. Eperon, S. K. Pathak, M. B. Johnston, A. Petrozza, L. Herz, H. Snaith, *Energy Environ. Sci.* **2014**, *7*, 3061.
[28] J. G. Tait, C. Wong, D. Cheyns, M. Turbiez, B. P. Rand, P. Heremans, *IEEE J. Photovoltaics* **2014**, *4*, 1538.
[29] N. Li, D. Baran, K. Forberich, M. Turbiez, T. Ameri, F. C. Krebs, C. J. Brabec, *Adv. Energy Mater.* **2013**, *3*, 1597.
[30] C. Girotto, D. Moia, B. P. Rand, P. Heremans, *Adv. Funct. Mater.* **2011**, *21*, 64.
[31] R. D. Deegan, O. Bakajin, T. F. Dupont, G. Huber, S. R. Nagel, T. A. Witten, *Nature* **1997**, *389*, 827.
[32] H. Hu, R. G. Larson, *J. Phys. Chem. B* **2006**, *110*, 7090.
[33] J. G. Tait, B. P. Rand, P. Heremans, *Org. Electron.* **2013**, *14*, 1002.
[34] Z. He, C. Zhong, S. Su, M. Xu, H. Wu, Y. Cao, *Nat. Photonics* **2012**, *6*, 593.